The Phoenix galaxy as seen by *NuSTAR*

A. Masini[1,2], A. Comastri[1], S. Puccetti[3,4], M. Baloković[5], P. Gandhi[6,7], M. Guainazzi[8,9], F. E. Bauer[10,11,12,13],
S. E. Boggs[14], P. G. Boorman[7], M. Brightman[5], F. E. Christensen[15], W. W. Craig[14,16], D. Farrah[17], C. J. Hailey[18],
F. A. Harrison[5], M. J. Koss[19], S. M. LaMassa[20], C. Ricci[10,13], D. Stern[21], D. J. Walton[21,22] and W. W. Zhang[20]

[1] INAF-Osservatorio Astronomico di Bologna, via Ranzani 1, 40127 Bologna, Italy
    e-mail: alberto.masini4@unibo.it
[2] Dipartimento di Fisica e Astronomia (DIFA), Università di Bologna, viale Berti Pichat 6/2, 40127 Bologna, Italy
[3] ASDC-ASI, Via del Politecnico, 00133 Roma, Italy
[4] INAF-Osservatorio Astronomico di Roma, Via Frascati 33, 00040 Monte Porzio Catone, Italy
[5] Cahill Center for Astronomy and Astrophysics, California Institute of Technology, Pasadena, CA 91125, USA
[6] Centre for Extragalactic Astronomy, Department of Physics, University of Durham, South Road, Durham DH1 3LE, UK
[7] School of Physics and Astronomy, University of Southampton, Highfield, Southampton SO17 1BJ, UK
[8] Institute of Space and Astronatical Science (JAXA), 3-1-1 Yoshinodai, Sagamihara, Kanagawa, 252-5252, Japan
[9] European Space Astronomy Center of ESA, P.O.Box 78, Villanueva de la Cañada, E-28691 Madrid, Spain
[10] Instituto de Astrofísica and Centro de Astroingeniería, Facultad de Física, Pontificia Universidad Católica de Chile, Casilla 306,
    Santiago 22, Chile
[11] Millennium Institute of Astrophysics (MAS), Nuncio Monseñor Sótero Sanz 100, Providencia, Santiago, Chile
[12] Space Science Institute, 4750 Walnut Street, Suite 205, Boulder, Colorado 80301
[13] EMBIGGEN Anillo, Concepción, Chile
[14] Space Science Laboratory, University of California, Berkeley, CA 94720, USA
[15] DTU Space National Space Institute, Technical University of Denmark, Elektrovej 327, 2800 Lyngby, Denmark
[16] Lawrence Livermore National Laboratory, Livermore, CA 94550, USA
[17] Department of Physics, Virginia Tech, Blacksburg, VA 24061, USA
[18] Columbia Astrophysics Laboratory, Columbia University, New York, NY 10027, USA
[19] Institute for Astronomy, Department of Physics, ETH Zurich, Wolfgang-Pauli-Strasse 27, CH-8093 Zurich, Switzerland
[20] NASA Goddard Space Flight Center, Greenbelt, MD 20771, USA
[21] Jet Propulsion Laboratory, California Institute of Technology, Pasadena, CA 91109, USA
[22] Space Radiation Laboratory, California Institute of Technology, Pasadena, CA 91125, USA

September 5, 2016

ABSTRACT

Aims. We study the long-term variability of the well-known Seyfert 2 galaxy Mrk 1210 (a.k.a. UGC 4203, or the Phoenix galaxy).
Methods. The source was observed by many X-ray facilities in the last 20 years. Here we present a *NuSTAR* observation and put the results in context of previously published observations.
Results. *NuSTAR* observed Mrk 1210 in 2012 for 15.4 ks. The source showed Compton-thin obscuration similar to that observed by *Chandra*, *Suzaku*, *BeppoSAX* and *XMM-Newton* over the past two decades, but different from the first observation by *ASCA* in 1995, in which the active nucleus was caught in a low flux state – or obscured by Compton-thick matter, with a reflection-dominated spectrum. Thanks to the high-quality hard X-ray spectrum obtained with *NuSTAR* and exploiting the long-term spectral coverage spanning 16.9 years, we can precisely disentangle the transmission and reflection components and put constraints on both the intrinsic long-term variability and hidden nucleus scenarios. In the former case, the distance between the reflector and the source must be at least ∼ 2 pc, while in the latter one the eclipsing cloud may be identified with a water maser-emitting clump.

Key words. X-rays: galaxies – galaxies: active – galaxies: Seyfert – galaxies: individual: Mrk 1210

1. Introduction

X-ray variability is a well-known property of active galactic nuclei (AGN). In recent years, many studies have focused on its characterization, and a class of extremely variable sources was found. Sources showing a transition between Compton-thin (i.e., with an obscuring column density of $10^{22} < N_{\rm H} < 10^{24}$ cm^{-2}) and Compton-thick levels of obscuration ($N_{\rm H} > 10^{24}$ cm^{-2}) are called "changing-look AGN", and are important to assess the relevance and physics of variability. The most famous cases are NGC 1365 (Risaliti et al. 2005; Walton et al. 2014; Rivers et al. 2015b), NGC 6300 (Guainazzi 2002), NGC 2992 (Gilli et al. 2000) , NGC 7674 (Bianchi et al. 2005, Gandhi et al. submitted), and NGC 7582 (Piconcelli et al. 2007; Rivers et al. 2015a). The nature of X-ray variability could be explained in different ways. A drop in flux can either be due to intrinsic fading of the central engine since we do not expect the accretion of matter on supermassive black holes (SMBHs) to be constant in time, or to an eclipsing phenomenon caused by some clumpy material absorbing the radiation along the line of sight (l.o.s.). There could be also other effects, like instabilities into the accretion flow. A significant change in the spectral shape with a constant flux can also occur.

In order to adequately study this complex property of AGN,

Table 1. History of X-ray observations of Mrk 1210.

| Instrument	Date of observation(s)
ASCA	1995-Oct-18, 1995-Nov-12
XMM-Newton	2001-May-5
BeppoSAX	2001-May-5
Chandra	2004-Mar-4
Swift	2006-Oct-6...2008-Apr-29 (4 times)
Suzaku	2007-May-2
Chandra	2008-Jan-15...2008-Feb-06 (5 times)
NuSTAR	2012-Oct-5

Fig. 1. Sloan Digital Sky Survey (SDSS) optical image of Mrk 1210 (gri composite). The cyan and red circles are the source extraction regions for the *NuSTAR* (see §2) and *Chandra* (see Appendix) spectra, respectively.

monitoring sources on a wide range of timescales, from weeks to years is needed, ideally with high sensitivity in the hard X-ray band (> 10 keV), which more directly probes the primary emission from the innermost regions of the AGN.

Mrk 1210 (z = 0.0135, Figure 1), also known as UGC 4203, hosts a Seyfert 2 AGN which was initially observed by *ASCA* in 1995 (Awaki et al. 2000). The flat spectrum and high equivalent width (EW) of the iron line at 6.4 keV were interpreted as emerging from reflection off circumnuclear matter of the AGN primary X-ray continuum, severely suppressed by Compton-thick absorption. In 2001, an *XMM-Newton* observation (Guainazzi et al. 2002) found that Mrk 1210, six years after the first observation, was still obscured but at the Compton-thin level only. Interpreting the change as an intrinsic flux enhancement, they coined the name "Phoenix galaxy" for this new changing-look AGN. Also Ohno et al. (2004), in the same year, observed Mrk 1210 with *BeppoSAX* and found similar results. Later on, the Phoenix galaxy was observed by other instruments, always showing variability of less than a factor of two in both intrinsic emission and column density, with the latter always in the Compton-thin regime (Matt et al. 2009; Risaliti et al. 2010). The list of all X-ray observations is presented in Table 1.

While the source has been extensively studied for the past twenty years, it is still not clear what is the reason for the changes observed between 1995 and 2001. A definitive answer is not yet available; however, as time went by, a change in $N_{\rm H}$ obscuring the nucleus was progressively addressed as the principal effect causing the change in flux. A better understanding of this source can be achieved thanks to the *Nuclear Spectroscopic Telescope Array* (*NuSTAR*). Launched in 2012, *NuSTAR* is the first telescope able to focus hard X-ray photons, enabling a gain of a factor ∼ 100 in sensitivity and one order of magnitude in angular resolution with respect to previous facilities in the hard (> 10 keV) X-ray band (Harrison et al. 2013). In its operating band (3–79 keV), thanks to a field of view (FoV) at 10 keV of 10′ × 10′, and an 18″ FWHM with a half-power diameter of 58″, *NuSTAR* is suitable for studying the hard X-ray spectra of AGN with high sensitivity. In this paper, we report on the *NuSTAR* observation of Mrk 1210 in 2012. After describing the data reduction (§2), we present the spectral analysis in §3. A discussion of our results in the context of the previous findings in the literature is provided in §4, and we draw our conclusions in §5.

2. Data reduction

NuSTAR observed Mrk 1210 on 2012 October 5 for 15.4 ks. The raw event file was processed using the *NuSTAR* Data Analysis Software package v. 1.5.1 (NuSTARDAS)[1]. Calibrated and

---

[1] http://heasarc.gsfc.nasa.gov/docs/nustar/analysis/nustar_swguide.pdf
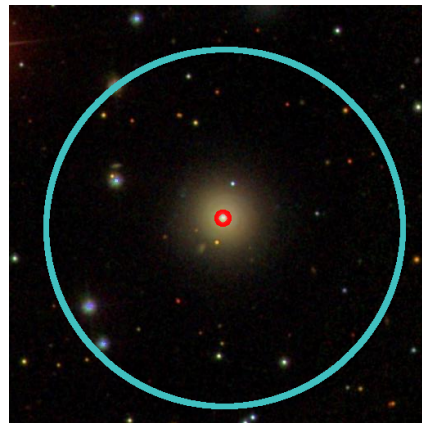
cleaned event files were produced using the calibration files in the *NuSTAR* CALDB (20150316) and standard filtering criteria with the `nupipeline` task. We used the `nuproducts` task included in the NuSTARDAS package to extract the *NuSTAR* source and background spectra using the appropriate response and ancillary files. We extracted the source spectrum and light curve in both focal plane modules, FPMA and FPMB, using 87″-radius circular apertures, while the background was extracted using three source-free circular regions on the same chip as the source. All spectra were binned to a minimum of 20 photons per bin using the HEAsoft task `grppha`.

3. Spectral analysis

We used the XSPEC software version 12.9.0 (Arnaud 1996) to carry out the spectral analysis. The source is clearly detected by *NuSTAR* up to ∼ 60 keV (Figure 2), with a net count rate of 0.3894 ± 0.0052 cts s^{-1} and 0.3762 ± 0.0052 cts s^{-1} for FPMA and FPMB, respectively. During the observation, the source kept a nearly constant flux, with amplitude variations of less than 30% and no systematic trend, as shown in Figure 3.

We included in all our fits a Galactic column density $N_{\rm H,gal}$ = 3.45×10^{20} cm^{-2} (Kalberla et al. 2005).

3.1. Phenomenological models

Since we know from previous work that a simple Galactic-absorbed power law is not able to reproduce the spectral complexity of Mrk 1210, we started fitting its spectrum with a `plcabs` model, a power law with an exponential cutoff, taking into account Compton scattering and absorption at the source (Yaqoob 1997). We also added a narrow (σ = 10 eV, fixed) Gaussian line component to fit the clearly visible feature at ∼ 6 keV. The fit was good (χ^2/ν = 537/480), with a photon index Γ = 1.40 ± 0.05 and an obscuring column of gas along the l.o.s. of $N_{\rm H}$ = (1.7 ± 0.2) × 10^{23} cm^{-2}. From previous studies, an additional soft component in the X-ray spectrum of the Phoenix galaxy is known (e.g., Guainazzi et al. 2002). Since this component can contribute between 3 and ∼ 5 keV in the *NuSTAR* band, we modeled it adding another power law, and linking all the parameters (photon index, redshift, normalization) to the ones of the `plcabs` component. We then allowed for a constant multiplicative value (referred to as $f_{\rm s}$) to vary in the fit, which rep-
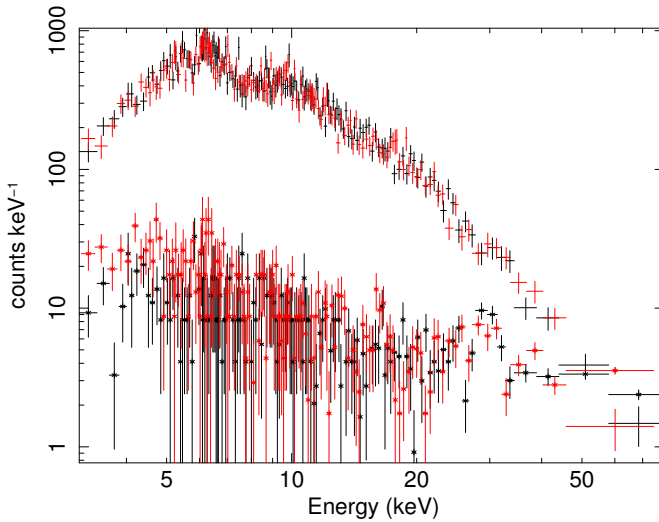
Fig. 2. *NuSTAR* background-subtracted spectrum of Mrk 1210 (FPMA in black, FPMB in red). The background is shown by diamonds, and is lower than the source signal up to ~ 50 keV. Both have been rebinned for plotting clarity.
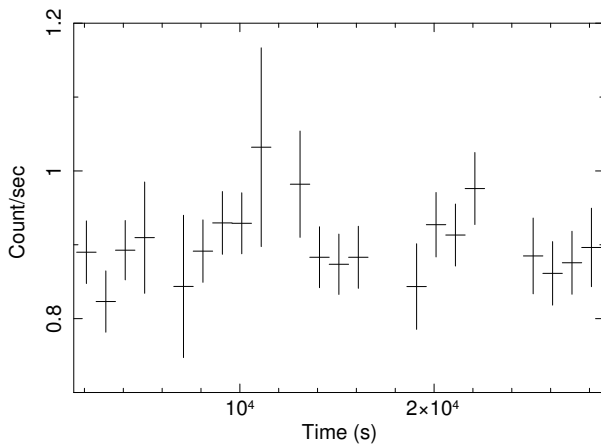

Fig. 3. 3-79 keV lightcurve of Mrk 1210. The background-subtracted FPMA and FPMB lightcurves were summed.

resents the fraction of the X-ray continuum Thomson-scattered into the soft X-rays. This procedure is often employed in the literature, and fractions of a few percent are typical (Bianchi & Guainazzi 2007). Adding a such scattered power law (SPL) improved the fit ($\chi^2/\nu = 521/479$) at more than a 99% confidence limit, based on an F-test.

Although the fit was already acceptable, we wanted to test if any reflection component was required by the data. We therefore added a `pexrav` model (Magdziarz & Zdziarski 1995), which includes Compton reflection on a slab of neutral material with infinite optical depth. The final model in XSPEC notation is the following:

$$\text{BASELINE} = \overbrace{\text{constant}}^{\text{cross-normalization}} \times \overbrace{\text{phabs}}^{\text{Gal. absorption}} \times$$
$$\times (\overbrace{\text{plcabs} + \text{pexrav} + \text{zgauss}}^{\text{nuclear emission}} +$$
$$+ \underbrace{f_s \times \text{zpowerlw}}_{\text{soft component (SPL)}}). \qquad (1)$$

We will refer to this as the "baseline" model. The fit improved dramatically ($\chi^2/\nu = 478/478$, $\Delta\chi^2 = 43$, see Figure 4): the

source had a photon index $\Gamma = 1.9 \pm 0.1$, a column density $N_H = 3.0^{+0.7}_{-0.6} \times 10^{23}$ cm^{-2}, a reflection parameter $R = 2.5^{+1.2}_{-0.9}$ (intended as the ratio of the `pexrav` normalization and the `plcabs` one) and a fraction of the primary power law scattered in the soft part of the spectrum of $8^{+5}_{-6}\%$, which is higher than the average of Seyfert 2 galaxies, but not unusual (Bianchi & Guainazzi 2007). However, this latter component is now only significant at the 97% confidence limit, due to the high level of reflection. Removing it, the fit gets slightly worse ($\chi^2/\nu = 483/479$), but the parameters are the same within the uncertainties.

We also note that the best fit line energy is lower than the iron Kα 6.4 keV centroid, although consistent with it at a 99% confidence limit (Figure 5). Using previous versions of the of the NuSTAR-DAS software (v 1.2.1) and *NuSTAR* CALDB (20130909), and applying the same baseline model, we find that all the fit parameters are the same within the uncertainties, with a centroid line energy of 6.35 ± 0.06 keV, which is now consistent with the expected value of 6.4 keV at a 90% confidence limit. Moreover, as we shall see in the next subsections (in particular in §3.3), we get good fits for the line feature adopting both toroidal models, in which the energy line is fixed to 6.4 keV, and a Compton shoulder is self-consistently calculated. Finally, since none of the previous observations found a such significant line energy shift, data with a better spectral resolution would be needed to assess the relevance of the one found here.

3.2. Toroidal models

The high reflection value obtained applying the baseline model implies a more complicated geometry or some time delay between the components; at the same time, a reflection component alone is not able to successfully fit the spectrum ($\chi^2/\nu = 609/481$). Therefore, we explored more physically motivated models which can take into account both absorption and reflection in a self-consistent way.

To this aim, we tried the BNTorus model (Brightman & Nandra 2011) and the MYTorus model (Murphy & Yaqoob 2009). They have been recently developed based on Monte Carlo simulations, adopting a toroidal geometry for the material responsible for obscuration, scattering, and line fluorescence, all self-consistently treated.

We first applied the BNTorus model to the data, fixing the inclination angle of the torus (i.e., the parameter θ_{inc}; $\theta_{\text{inc}} = 0$ describes a face-on view) to 87°. The fit was acceptable ($\chi^2/\nu = 517/481$), with $\Gamma = 1.57^{+0.10}_{-0.06}$, $N_H = 2.8^{+0.7}_{-0.5} \times 10^{23}$ cm^{-2}, and half-opening angle of the torus $\theta_{\text{tor}} < 65°$, from which a covering factor of > 0.4 is inferred. A very high fraction, $16^{+4}_{-5}\%$, of the primary power law is scattered below 5 keV.

Similarly, the MYTorus model in its "coupled", default mode (i.e. with a donut-shaped, smooth reprocessor with a covering factor of 0.5) gives an acceptable fit: $\chi^2/\nu = 512/480$, $\Gamma = 1.63 \pm 0.08$, $N_H = (3.5 \pm 0.6) \times 10^{23}$ cm^{-2}, with a high fraction, $(12 \pm 3)\%$, of the primary power law scattered below 5 keV. However, using either torus model, the spectrum is still too peaky at $\sim 30-40$ keV (see Figure 6), and we conclude that they are not able to capture the spectral shape of Mrk 1210 while the phenomenological, baseline model does. This suggests that the Mrk 1210 torus contains Compton-thick material producing the pronounced Compton hump, but our line of sight does not pass the Compton-thick part in the *NuSTAR* observation.
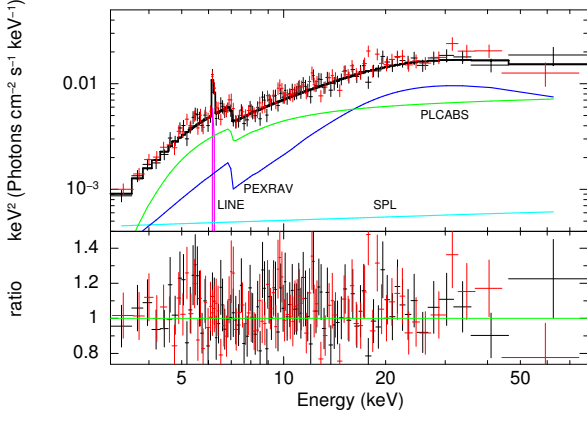
Fig. 4. Fit with the baseline model (1) to the *NuSTAR* spectrum of Mrk 1210 (FPMA in black, FPMB in red).
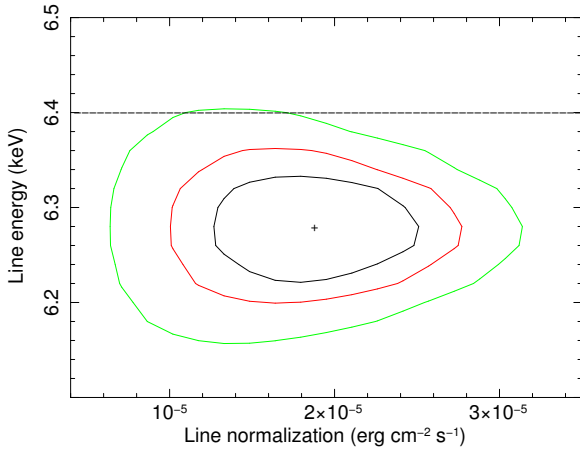

Fig. 5. 68% (black), 90% (red), 99% (green) confidence contours. The two-dimensional confidence contours allow a marginal consistency with the iron Kα line at 6.4 keV, indicated with the dashed horizontal line.

3.3. A physical picture

In the previous Section we found that the reflection component, modeled with a `pexrav` model, has a normalization a factor $\sim 2.5\times$ larger than the primary continuum from the AGN. Indeed, applying other self-consistent models based on Monte Carlo simulations with a classic toroidal geometry, we found worse fits with respect to that obtained with the baseline model, due to the presence of the reflection excess.

While the BNTorus model allows the user to fit for the torus opening angle and hence to get an estimate of the covering factor of the source, the three components of the MYTorus model can be decoupled (transmitted flux, reflected flux, and fluorescence lines) to simulate different – and more complex – geometries (we refer to Yaqoob 2012 for an extensive explanation of the decoupled version of the model, but see also LaMassa et al. 2014 for a systematic application of the model on a sample of sources). Briefly, together with the canonical components with a l.o.s. angle fixed at 90°(called front-scattered, with the subscript 90), the decoupled version includes an additional couple of scattered+line components seen "face on", i.e. with the l.o.s. angle fixed to 0°(called back-scattered, with the subscript 00). The relative normalizations between the 90°and 0°components (called
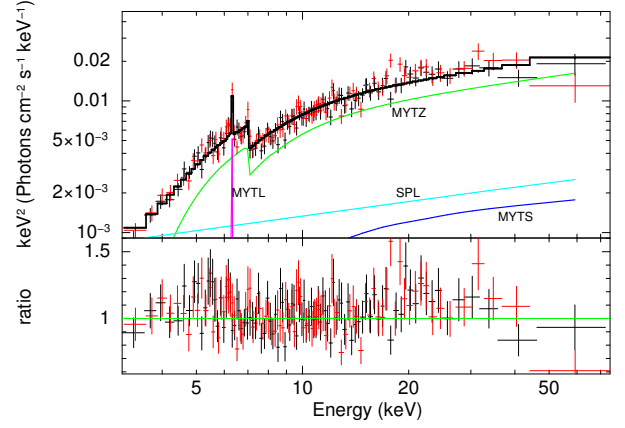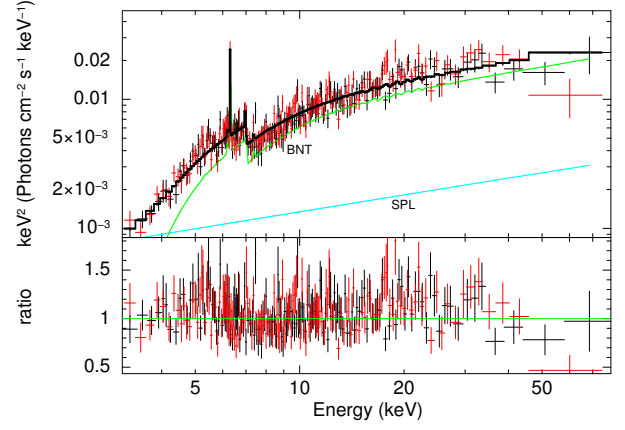
Fig. 6. Fit with with the BNTorus model (top) and the coupled MYTorus model (bottom) to the *NuSTAR* spectrum of Mrk 1210 (FPMA in black, FPMB in red).

A_{S90} and A_{S00}, respectively) can be untied and left free in the fit. Additionally, one can also untie the column densities of the two scattered/reflected components. In XSPEC notation, this model is described as

$$\text{MYT\_DEC} = \overbrace{\text{constant}}^{\text{cross-normalization}} \times \overbrace{\text{phabs}}^{\text{Gal. absorption}} \times$$

$$\times (\overbrace{\text{zpowerlw} \times \text{MYTZ}}^{\text{absorption}} + \overbrace{\text{MYT}_{S,90} + \text{MYT}_{L,90}}^{\text{front-scattering}} +$$

$$+ \overbrace{\text{MYT}_{S,00} + \text{MYT}_{L,00}}^{\text{back-scattering}} + \overbrace{f_s \times \text{zpowerlw}}^{\text{soft component (SPL)}}). \quad (2)$$

If we decouple the model (i.e., we leave free the constants A_{S90} and A_{S00}), and allow the obscuring columns to be different (i.e., $N_{H90} \neq N_{H00}$), we get a good fit ($\chi^2/\nu = 489/479$, Figure 7), The front-scattered component vanishes (i.e., $A_{S90} \rightarrow 0$), while the back-scattered component converges to the same normalization as the primary continuum (i.e., $A_{S00} \rightarrow 1$, preserving the internal self-consistency of the model), and the clouds responsible for the reflection component are Compton-thick, with an optical depth $\tau \sim 2.7$ ($N_H \sim 4 \times 10^{24}$ cm^{-2}). Moreover, the upper limit on the column density is unconstrained by the fit. In other words, the column density obscuring the l.o.s. is different from the column density of the clouds responsible of the back-scattered reflection. Fixing the normalizations of the back-scattered component and the primary power law to be equal as suggested by the fit (i.e., $A_{S00} = 1$), does not change the result regarding the different column densities for the two components. On the other hand,

Table 2. Summary of spectral analysis.

Parameter	Models		
	BASELINE	MYT[*]	MYT decoupled
χ^2/ν	478/478	512/480	489/479
Γ	$1.90^{+0.11}_{-0.12}$	$1.63^{+0.08}_{-0.07}$	1.85 ± 0.12
$N_{\rm H}$ [cm^{-2}]	$3.0^{+0.7}_{-0.6} \times 10^{23}$	$3.5^{+0.6}_{-0.6} \times 10^{23}$	$3.3^{+0.8}_{-0.7} \times 10^{23}$
Norm transmitted comp @1 keV [ph cm^{-2} s^{-1} keV^{-1}]	$5.1^{+1.3}_{-1.0} \times 10^{-3}$	$4.8^{+1.3}_{-1.1} \times 10^{-3}$	$7.8^{+3.8}_{-2.6} \times 10^{-3}$
Norm reflected comp @1 keV [ph cm^{-2} s^{-1} keV^{-1}]^a	$1.2^{+0.9}_{-0.5} \times 10^{-2}$	4.8×10^{-3} (fixed)	$7.7^{+5.1}_{-3.1} \times 10^{-3}$
$N_{\rm H00}$ [cm^{-2}]^b			$4.0^{+u}_{-1.6} \times 10^{24}$
Line Energy [keV]	$6.28^{+0.06}_{-0.07}$		
EW Line [eV]	141 ± 50		
Norm line component (flux) [ph cm^{-2} s^{-1}]	$(1.9 \pm 0.7) \times 10^{-5}$		
$f_{\rm s}$ [%]	8^{+5}_{-6}	12^{+3}_{-2}	8^{+3}_{-2}
F_{2-10} [erg cm^{-2} s^{-1}]	7.6×10^{-12}	7.8×10^{-12}	7.7×10^{-12}
F_{10-40} [erg cm^{-2} s^{-1}]	3.0×10^{-11}	2.9×10^{-11}	3.0×10^{-11}
$L^{\rm int}_{2-10}$ [erg s^{-1}]	6.0×10^{42}	8.6×10^{42}	1.0×10^{43}
$L^{\rm int}_{10-40}$ [erg s^{-1}]	6.1×10^{42}	1.3×10^{43}	1.1×10^{43}
FPMB/FPMA	1.05 ± 0.03	1.05 ± 0.03	1.05 ± 0.03

Notes. The values of the fluxes reported in the table are the observed ones, while those of the luminosities are intrinsic, i.e. deabsorbed. $^{(*)}$ The results using a BNTorus model are the same within the uncertainties, and the main parameters of the fit are described in the text. We chose to show the MYTorus results to facilitate comparison between the coupled and decoupled cases. $^{(a)}$ The reflection component is the `pexrav` model in the first column. In the coupled configuration of MYTorus, absorption, fluorescence and reflection are self-consistently treated. For this reason, only one normalization is needed to describe all the components (second column). In the last column, the reflection is instead made up by the back-scattered MYTorus component, namely MYTS,00. $^{(b)}$ The column density is associated with the back-scattered reflection component in the decoupled MYTorus model, MYTS,00. .
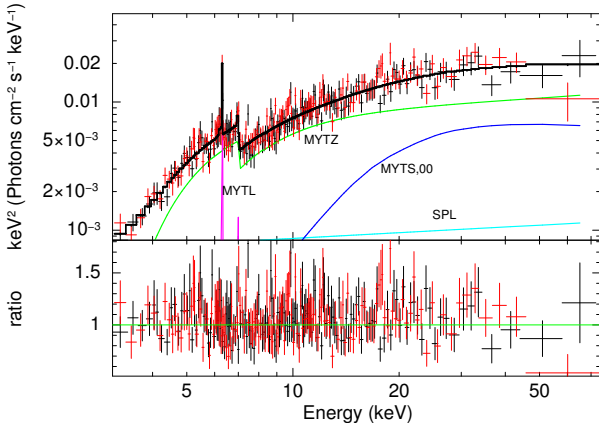

Fig. 7. Fit with the MYTorus decoupled model (2), with normalizations and column densities decoupled (FPMA in black, FPMB in red). Fitting parameters are reported in Table 2.

a worse fit is obtained ($\chi^2/\nu = 505/479$, $\Delta\chi^2 = 16$ for the same number of degrees of freedom) if the reflection component is front-scattered, i.e., if we simply decouple the column densities from the default configuration of MYTorus. Also in this case, the data require two different absorbing columns: a Compton-thin one obscuring the primary emission, and a thick one producing the reflection. The parameters of the models used for fitting (baseline, toroidal, MYTorus decoupled) are shown in Table 2.

3.4. Intrinsic luminosity

Our models find an intrinsic 2–10 keV luminosity in the range $0.6 - 1 \times 10^{43}$ erg s^{-1}. It is interesting to compare these results with other commonly used proxies for the X-ray luminosity. Using the mid-infrared luminosity, the *WISE* all-sky catalog (Wright et al. 2010; Cutri et al. 2013) reports a $W3$ (12 μm) magnitude of 4.634 ± 0.015, which translates to a 12 micron luminosity $L_{12\mu m} = 4.6 \times 10^{43}$ erg s^{-1}, with a $\sim 1.5\%$ statistical error, using the standard *WISE* zeropoints. The $W1 - W2$ color is 1.392 ± 0.030, suggesting that the mid-infrared luminosity is AGN-dominated, being the source above the color threshold of $W1 - W2 > 0.8$ identified by Stern et al. (2012). Then, from the mid-IR/X-ray relation (Gandhi et al. 2009; Asmus et al. 2015), one would predict $\log(L_{2-10}[\text{erg/s}]) \sim 43.3$, which is consistent with our MYTorus luminosity.

We can also use the optical [OIII] emission line to provide another independent estimate of the X-ray luminosity. Koss et al. (submitted) report a dust reddening-corrected [OIII]λ5007 flux of $F^c_{\rm [OIII]} \sim 8.03 \times 10^{-13}$ erg cm^{-2} s^{-1}, from which we derive a luminosity of $L_{\rm [OIII]} \sim 3.0 \times 10^{41}$ erg s^{-1}. Using the relationship for Seyfert galaxies between L_{2-10} and $L_{\rm [OIII]}$ with a scatter of 0.5 dex presented in Berney et al. (2015), we predict $\log(L_{2-10}[\text{erg/s}]) \sim 43.3$, consistent with the luminosity derived from the infrared and with that obtained by our spectral analysis. These values suggest that the luminosity derived by the "baseline" model is likely underestimated of a factor ~ 2, due to the phenomenological combination of the absorbed power law and infinite slab reflection models. The physically motivated decoupled MYTorus model alleviates this problem and allows a more reliable estimate of the intrinsic luminosity of the source.
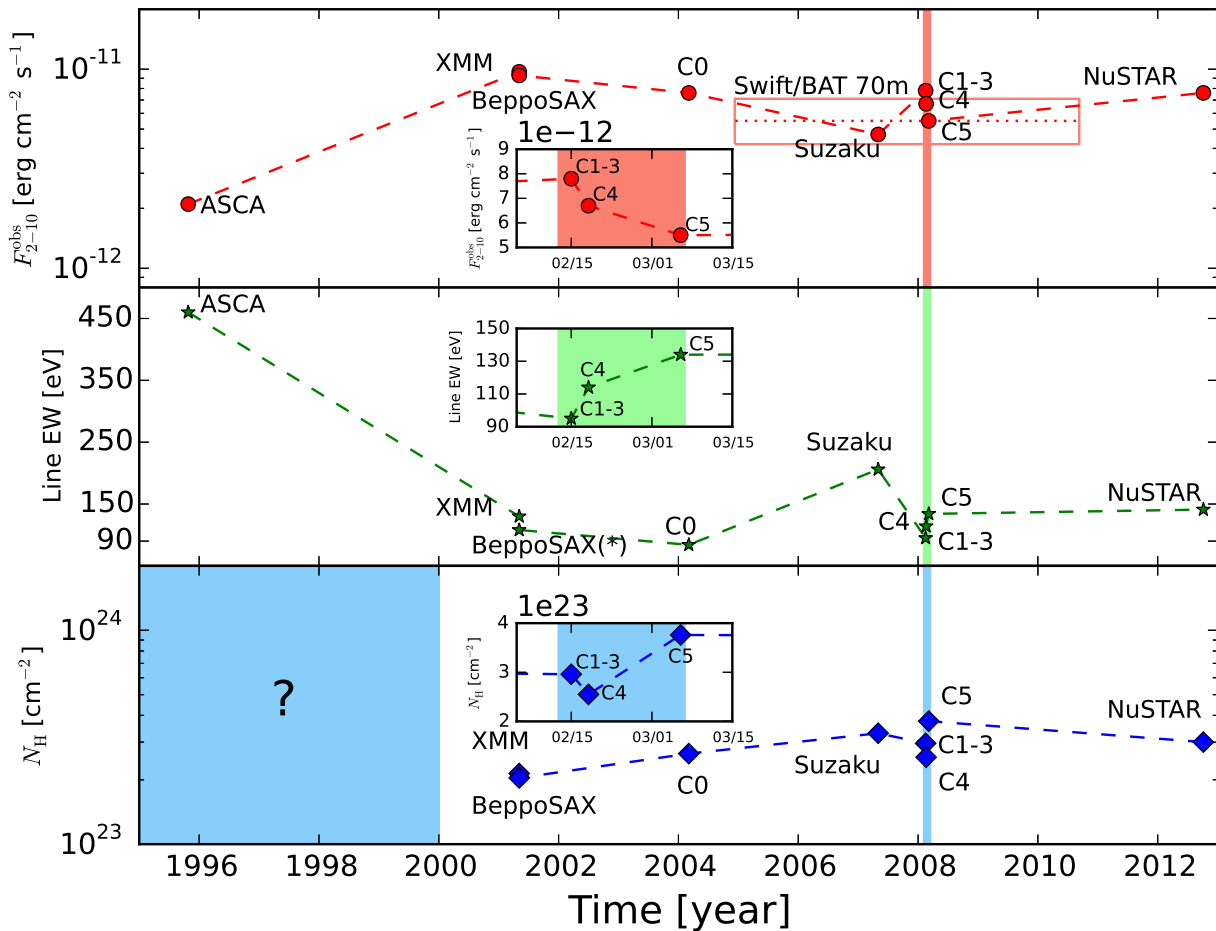
Fig. 8. Observed flux in the 2−10 keV band of Mrk 1210 (top panel), Fe Kα line equivalent width (middle panel) and column density (bottom panel) as a function of time. The inset panels show the zoomed-in region of the five *Chandra* observations during 2008. (*) We report here the equivalent width of model 1 instead of that of model 2 in Ohno et al. (2004). The two values are consistent within the uncertainties, and we adopt the more constrained one for clarity.

4. Long-term behavior and discussion

In order to understand the time dependent variation of the X-ray spectrum, we compiled the observed 2−10 keV fluxes, iron line equivalent widths, and column densities from the literature together with results of this work, to have a global picture of the behavior of the source. We choose to use our "baseline" model parameters (shown in Table 2) in order to compare directly with the results from previous papers based on the same phenomenological models. To do so, we reduced the data of the six *Chandra* observations with standard procedures. See the Appendix for the analysis of the 2004 observation (hereafter "C0"), while for the other five observations during 2008 (namely, "C1-5") the best-fitting models of Risaliti et al. (2010), analogous to our baseline model, were applied. We also note that Mrk 1210 is bright enough to be detected by the Burst Alert Telescope (BAT) onboard *Swift*, and it is indeed present in the *Swift*/BAT 70 month catalog (Baumgartner et al. 2013). As can be easily seen from the top panel of Figure 8, the source was in a low-flux state during the *ASCA* observation. It has been seen in a high-flux state since then, with different observatories. The equivalent widths of the iron line (Figure 8, middle panel) reflect this trend. From

the bottom panel of Figure 8 it is clear that the column density of the source has been around $2 - 4 \times 10^{23}$ cm^{-2} since 2001, while the *ASCA* data do not help in shedding light on the column density in 1995. Both Awaki et al. (2000) and Guainazzi et al. (2002) found a Compton-thin obscuration applying a pure transmission model to the *ASCA* data, despite getting a worse fit with respect to a reflection-dominated scenario. On the other hand, the absorption-corrected 2−10 keV luminosity reported by Awaki et al. (2000) is a factor of ∼ 5 lower than the later intrinsic luminosities, but the quality of the data does not allow a robust estimate of the intrinsic luminosity, nor a robust detection of the transmitted continuum, leaving total degeneracy between heavily absorbed and intrinsically faint primary emission scenarios. In the following, both the flux change (§4.1) and the eclipsing scenario (§4.2) are discussed.

4.1. Change in intrinsic luminosity

If we suppose that Mrk 1210 was Compton-thin also during the *ASCA* observation, but with the intrinsic emission shut off, the reflection-dominated spectrum was entirely due to an echo of a previous high-flux state.

Table 3. *ASCA* best fit parameters compared with *NuSTAR* `pexrav+zgauss` only model.

Parameter	*ASCA*	*NuSTAR* (pexrav+line)
Γ	$1.95^{+0.45}_{-0.40}$	$1.90^{+0.11}_{-0.12}$
Line EW [eV]	460 ± 210	484
F_{2-10} [cgs]	1.8×10^{-12}	2.3×10^{-12}
L^{int}_{2-10} [cgs]	2.3×10^{42}	0.9×10^{42}

Notes. The *NuSTAR* line equivalent width is calculated with respect to the reflection continuum.
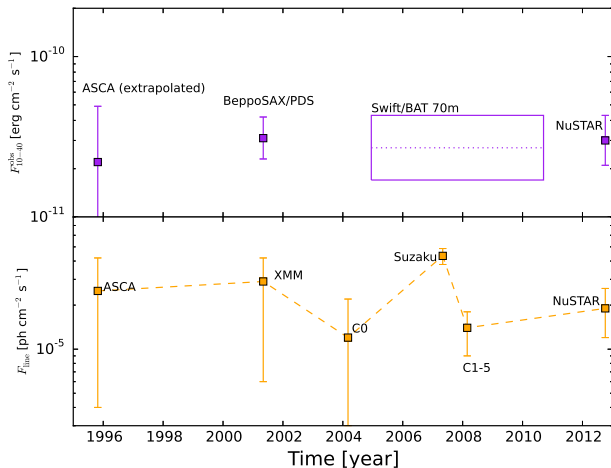
Fig. 9. Observed $10-40$ keV flux (top panel) and iron line flux (bottom panel) of Mrk 1210, as a function of time.

Thanks to the high-quality *NuSTAR* spectrum, we are able to disentangle the intrinsic power law and the reflection component. If we shut off the intrinsic component in our *NuSTAR* data, leaving only the `pexrav` model and the line component (i.e., a reflection dominated model), we find an observed flux and line equivalent width consistent with the values reported by Awaki et al. (2000), albeit uncertainties on these values cannot be reliably computed, being a reflection dominated scenario highly disfavored by the *NuSTAR* data, as already discussed in §3 (see Table 3). Moreover, from the *NuSTAR* best fit baseline model, we can easily adjust the fit parameters, and vary only the normalization of the intrinsic continuum, to recover all the subsequent states of Mrk 1210, which are similar to the *NuSTAR* one. This means that keeping a reflection component constant and varying only the intrinsic continuum, together with minor – a factor ~ 2, but required – column density variations on shorter timescales (as noted by Risaliti et al. 2010), all the observations of the Phoenix galaxy during the last ~ 20 years can be explained. As a further check, the 10–40 keV observed flux and line flux are plotted in Figure 9. In the top panel, we computed the 10–40 keV flux, which is the band where the reflection component is thought to dominate, from *BeppoSAX*/PDS[2], *Swift*/BAT 70 month catalog[3], and *NuSTAR*. We also extrapolated the *ASCA* 10–40 keV flux, using the same procedure of *Swift*/BAT. The bottom panel

shows the line flux for the iron line component, measured by different instruments. Both panels seem to confirm the constancy of the reflection through years, with a hint of a slightly enhanced line during the *Suzaku* observation.

If this is the correct picture, Mrk 1210 turned on between 1995 and 2001, and stayed more or less constant since then. The reflection component, though, still has to adjust and respond to this change, since it can be considered constant between all the observations. A simple light-travel argument can then put constraints on the distance between the central source and the reflector. For an edge-on view of the system, $D = c\Delta t/2$, and $\Delta t > 12 - 17$ yr, depending on when the source switched on (between the beginning of 1996 and the beginning of 2001). In this case, the distance between the source and the reflector is $D > (1.9 - 2.6)$ pc. First a fading, and then an increase in reflection is then expected to occur in the future, and monitoring of the source is the only way to keep track of its changes. Monitoring could also shed new light on the role of the X-ray absorber, which varies on much shorter temporal scales and seems to be associated with broad line region (BLR) clouds (see Risaliti et al. 2010). If this is the case, the physical interpretation of our result applying the decoupled MYTorus model is straightforward: the l.o.s. is intercepting the variable (and presumably compact) Compton-thin absorber, while the reflector is located on larger scales and the photons reflecting back to our l.o.s. are "seeing" a Compton-thick column of gas. Risaliti et al. (2010) suggest that the absorber is a BLR cloud, assuming a central black hole (BH) mass of $5 - 7 \times 10^7 M_\odot$. In this picture, a second "screen" is required to obscure the broad lines in the optical spectrum, which is instead likely showing an outflow, resulting in the classification of Mrk 1210 as a Seyfert 2 (Mazzalay & Rodríguez-Ardila 2007). However, if the reflection component comes from photons reflecting off the far inner wall of the torus, delayed with respect to the intrinsic emission, a rather distant torus edge is needed with respect to the dust sublimation radius R_{sub}, which is usually thought to mark the inner wall of the torus, and in this case is ~ 0.2 pc (Gandhi et al. 2009 and references therein, and adopting a bolometric correction of 20, Lusso et al. 2012).

4.2. Eclipsing event

The *ASCA* data cannot distinguish between a Compton-thick eclipsing event and an intrinsic low-flux state of the central engine. A random pass of a Compton-thick cloud (or an alignment of clouds along the l.o.s.) during the *ASCA* observation is consistent with the known clumpiness of the gas surrounding obscured AGN. During the two observations by *ASCA* in 1995, separated by 25 days, Mrk 1210 was in a low-flux state. In an eclipsing scenario, this means that the putative eclipsing event lasted for at least 25 days. Assuming Keplerian motion of the clump, the linear size eclipsed by a moving Compton-thick cloud in a given time interval can be written as $s = 4.5 \times 10^{13} (M_7/D_{pc})^{1/2} \Delta t_{25}$ cm, where D_{pc} is the distance from the center in parsecs, and Δt_{25} is the eclipse time interval in units of 25 days. This implies that the cloud is rotating with a Keplerian velocity $v_K \sim 210 (M_7/D_{pc})^{1/2}$ km/s. Finally, assuming a Compton-thick column density the average density of the clump is $\rho \sim 2 \times 10^{10} N_{H,24} (D_{pc}/M_7)^{1/2}/\Delta t_{25}$ cm^{-3}, where $N_{H,24}$ is the column density in units of 10^{24} cm^{-2}. Interestingly, high-density clumps on a parsec-scale (or subparsec-scale) are observed in some systems showing water maser emission at 22 GHz. Mrk 1210 is indeed one of them (Braatz et al. 1994), even if the association of the maser spots to a particular geometry is still

---

unclear and sensitive VLBI observations are needed to further investigate the nuclear environment. The maser activity could indeed be associated with a dusty Keplerian disk orbiting the SMBH, from which the most precise BH mass available to date could be derived (e.g. Kuo et al. 2011). This would allow a direct comparison of this object with other samples of disk masers (Pesce et al. 2015; Masini et al. 2016) and get clues on the X-ray absorber. On the other hand, the maser spots could either be associated with the outflow seen in the optical spectrum, invalidating any possible BH mass estimate. Moreover, as reported by Storchi-Bergmann et al. (1998) and Mazzalay & Rodríguez-Ardila (2007), Mrk 1210 probably shows a recent circumnuclear starburst. If the masers are associated with the outflow responsible for the broad components of the optical lines, the Phoenix galaxy could be a very interesting and local laboratory to study the interplay between AGN activity and star formation.

5. Conclusions

We presented the first *NuSTAR* observation of Mrk 1210, also known as the Phoenix galaxy. It is a long-studied object, considered to be part of the "changing-look" class of AGN. *NuSTAR* observed Mrk 1210 obscured by a Compton-thin column of gas, like other instruments over the past 16 years. The data are also showing an enhanced reflection component, which requires two different columns of gas to be taken into account. Many previous studies have suggested the presence of a variable X-ray absorber, inducing changes in absorbing column of a factor ~ 2 on the timescales of days and weeks. We note that these short-term column changes, properly complemented by long-term intrinsic variability of the central engine, are able to explain the line equivalent widths and fluxes observed by different instruments during the last ~ 20 years. If the low flux-state observed by *ASCA* in 1995 is due to an intrinsic fading of the engine, we note evidence that the reflection component has remained constant with time. In this scenario, we infer that the physical distance between the source and the reflector is of the order of at least 2 pc. First a drop, and then an enhancement of the reflection component are then expected to occur in the future, in response of the source "low-flux state" (seen by *ASCA*) and soft X-ray "awakening" (i.e. the "Phoenix effect", Guainazzi et al. 2002) seen between 1996 and 2001. On the other hand, if the low-flux state of Mrk 1210 during the *ASCA* observation can be ascribed to the presence of a Compton-thick cloud obscuring the l.o.s., the cloud can be identified with a maser-emitting clump on the sub-pc scale. Indeed, if the torus-like structure is clumpy, a random passage of an over-dense cloud along the l.o.s. is expected (Wada 2012). The frequency in which such events are to be expected could be evaluated with precise hydrodynamical simulations of the nuclear environment, but see Markowitz et al. (2014) for a statistical study on this topic.

Monitoring in the X-ray band is needed, either to detect the expected behavior of the reflection component and clarify the relation between the X-ray absorber and reflector, which seem to be on different spatial scales, or to possibly detect another low-flux state and further study the properties of the clumpy (sub)pc-scale absorber. To this extent, radio VLBI monitoring at 22 GHz would also be extremely useful to clarify the nature of the nuclear water maser activity.

References

Arnaud, K. A. 1996, in Astronomical Society of the Pacific Conference Series, Vol. 101, Astronomical Data Analysis Software and Systems V, ed. G. H. Jacoby & J. Barnes, 17

Asmus, D., Gandhi, P., Hönig, S. F., Smette, A., & Duschl, W. J. 2015, MNRAS, 454, 766

Awaki, H., Ueno, S., Taniguchi, Y., & Weaver, K. A. 2000, ApJ, 542, 175

Baumgartner, W. H., Tueller, J., Markwardt, C. B., et al. 2013, ApJS, 207, 19

Berney, S., Koss, M., Trakhtenbrot, B., et al. 2015, MNRAS, 454, 3622

Bianchi, S. & Guainazzi, M. 2007, in American Institute of Physics Conference Series, Vol. 924, The Multicolored Landscape of Compact Objects and Their Explosive Origins, ed. T. di Salvo, L. Israel, L. Piersant, L. Burderi, G. Matt, A. Tornambe, & M. T. Menna, 822–829

Bianchi, S., Guainazzi, M., Matt, G., et al. 2005, A&A, 442, 185

Braatz, J. A., Wilson, A. S., & Henkel, C. 1994, ApJ, 437, L99

Brightman, M. & Nandra, K. 2011, MNRAS, 413, 1206

Cutri, R. M., Wright, E. L., Conrow, T., et al. 2013, Explanatory Supplement to the AllWISE Data Release Products, Tech. rep.

Gandhi, P., Horst, H., Smette, A., et al. 2009, A&A, 502, 457

Gilli, R., Maiolino, R., Marconi, A., et al. 2000, A&A, 355, 485

Guainazzi, M. 2002, MNRAS, 329, L13

Guainazzi, M., Matt, G., Fiore, F., & Perola, G. C. 2002, A&A, 388, 787

Harrison, F. A., Craig, W. W., Christensen, F. E., et al. 2013, ApJ, 770, 103

Kalberla, P. M. W., Burton, W. B., Hartmann, D., et al. 2005, A&A, 440, 775

Kuo, C. Y., Braatz, J. A., Condon, J. J., et al. 2011, ApJ, 727, 20

LaMassa, S. M., Yaqoob, T., Ptak, A. F., et al. 2014, ApJ, 787, 61

Lusso, E., Comastri, A., Simmons, B. D., et al. 2012, MNRAS, 425, 623

Magdziarz, P. & Zdziarski, A. A. 1995, MNRAS, 273, 837

Markowitz, A. G., Krumpe, M., & Nikutta, R. 2014, MNRAS, 439, 1403

Masini, A., Comastri, A., Baloković, M., et al. 2016, A&A, 589, A59

Matt, G., Bianchi, S., Awaki, H., et al. 2009, A&A, 496, 653

Mazzalay, X. & Rodríguez-Ardila, A. 2007, A&A, 463, 445

Murphy, K. D. & Yaqoob, T. 2009, MNRAS, 397, 1549

Ohno, M., Fukazawa, Y., & Iyomoto, N. 2004, PASJ, 56, 425

Pesce, D. W., Braatz, J. A., Condon, J. J., et al. 2015, ApJ, 810, 65

Piconcelli, E., Bianchi, S., Guainazzi, M., Fiore, F., & Chiaberge, M. 2007, A&A, 466, 855

Risaliti, G., Elvis, M., Bianchi, S., & Matt, G. 2010, MNRAS, 406, L20

Risaliti, G., Elvis, M., Fabbiano, G., Baldi, A., & Zezas, A. 2005, ApJ, 623, L93

Rivers, E., Baloković, M., Arévalo, P., et al. 2015a, ApJ, 815, 55

Rivers, E., Risaliti, G., Walton, D. J., et al. 2015b, ApJ, 804, 107

Stern, D., Assef, R. J., Benford, D. J., et al. 2012, ApJ, 753, 30

Storchi-Bergmann, T., Fernandes, R. C., & Schmitt, H. R. 1998, ApJ, 501, 94

Wada, K. 2012, ApJ, 758, 66

Walton, D. J., Risaliti, G., Harrison, F. A., et al. 2014, ApJ, 788, 76

Wright, E. L., Eisenhardt, P. R. M., Mainzer, A. K., et al. 2010, AJ, 140, 1868

Yaqoob, T. 1997, ApJ, 479, 184
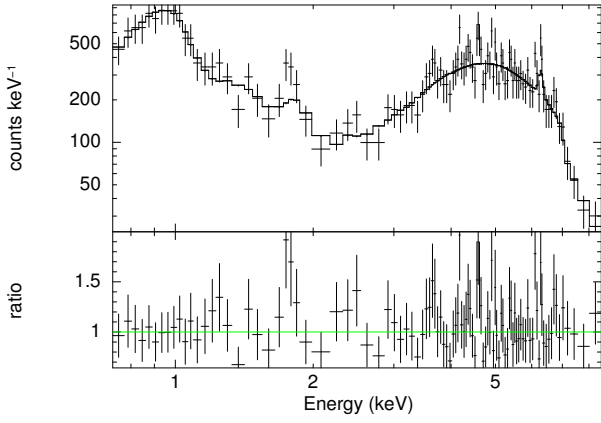
Yaqoob, T. 2012, MNRAS, 423, 3360

Fig. A.1. Best fit and data/model ratio to the 2004 *Chandra* spectrum of Mrk 1210.

Appendix A: Analysis of the *Chandra* 2004 (C0) observation

We reduced the *Chandra* data and produced a grouped spectrum using the CIAO standard `chandra_repro` and `specextract` tasks. The source counts were extracted from a 3″-radius circular region, while the background was extracted from four 10″ circular regions. Soft X-ray emission below 3 keV is clearly present in the total spectrum (Figure A.1), and was fitted, following Risaliti et al. (2010), with an `apec+zpowerlw` model. The hard X-ray part of the spectrum was fitted with our "baseline" model, Equation (1). The fitting parameters are reported in Table A.1. We note that the results are consistent with the *NuSTAR* observation presented in the paper.

Table A.1. C0 observation; best fitting parameters.

Parameter	Value
χ^2/ν	83/95
Hard component	
Γ	$1.56^{+0.58}_{-0.63}$
N_H [cm^{-2}]	$2.7^{+0.8}_{-1.0} \times 10^{23}$
Norm transmitted comp @1 keV [ph cm^{-2} s^{-1} keV^{-1}]	$2.2^{+6.9}_{-1.7} \times 10^{-3}$
Norm reflection comp @1 keV [ph cm^{-2} s^{-1} keV^{-1}]	$1.2^{+1.0}_{-1.0} \times 10^{-2}$
Line Energy [keV]	$6.36^{+0.08}_{-0.21}$
EW Line [eV]	84^{+74}_{-68}
Norm line component (flux) [ph cm^{-2} s^{-1}]	$1.2^{+1.0}_{-1.0} \times 10^{-5}$
Soft component	
kT [keV]	$1.02^{+0.16}_{-0.09}$
Norm `apec` @1 keV [ph cm^{-2} s^{-1} keV^{-1}]	$4.3^{+1.4}_{-1.3} \times 10^{-5}$
Γ_s	3.0^{+u}_{-l}
Norm `zpowerlw` @1 keV [ph cm^{-2} s^{-1} keV^{-1}]	$2.9^{+2.9}_{-2.9} \times 10^{-5}$
F_{2-10} [erg cm^{-2} s^{-1}]	7.6×10^{-12}